NUCLEAR THEORY, Vol. 35 (2016)
eds. M. Gaidarov, N. Minkov, Heron Press, Sofia

Deformed Shell Model Study of Heavy N=Z Nuclei and Dark Matter Detection

R. Sahu[1], **V.K.B. Kota**[2]

[1]Physics Department, Berhampur University, Berhampur-760007, Odisha, India.

[2]Physical Research Laboratory, Ahmedabad-380009, India.

Abstract. Deformed shell model (DSM) based on Hartree-Fock intrinsic states is applied to address two current problems of interest. Firstly, in the $f_{5/2}pg_{9/2}$ model space with jj44b effective interaction along with isospin projection, DSM is used to describe the structure of the recently observed low-lying $T = 0$ and $T = 1$ bands in the heavy odd-odd N=Z nucleus ^{66}As. DSM results are close to the data and also to the shell model results. For the $T = 1$ band, DSM predicts structural change at 8^+ just as in the shell model. In addition, the lowest two $T = 0$ bands are found to have quasi-deuteron structure above a ^{64}Ge core and the 5^+ and 9^+ levels of the third $T = 0$ band are found to be isomeric states. Secondly, in a first application of DSM to dark matter, detection rates for the lightest supersymmetric particle (a dark matter candidate) are calculated with ^{73}Ge as the detector.

1 Introduction

There has been considerable interest in investigating the structure of the nuclei in the mass region $A = 60 - 100$ and in particular odd-odd $N = Z$ nuclei as these nuclei are expected to give new insights into neutron-proton (np) correlations that are hitherto unknown. The N=Z nuclei in this mass region lie near the proton drip-line. With the development of radioactive ion beam facilities and large detector arrays, new experimental results for the energy spectra of ^{62}Ga [1], ^{66}As [2], ^{70}Br [3], ^{74}Rb [4], ^{78}Y [5], ^{82}Nb [6] and ^{86}Tc [6] have opened up challenges in developing models for describing and predicting the spectroscopic properties of these nuclei. On the other hand, many interesting phenomena have been observed with shape changes and delayed alignments in even-even $N = Z$ nuclei from ^{64}Ge to ^{88}Ru. For example, ^{64}Ge exhibits γ-soft structure [7], ^{68}Se exhibits oblate shape in the ground state [8], ^{72}Kr [9–11] exhibits shape coexistence, ^{76}Sr and ^{80}Zr have large ground state deformations [12, 13] and so on. Recently, evidence for a spin-aligned np isoscalar paired phase has been reported from the level structure of ^{92}Pd [14]. Also many even-even $N = Z$ nuclei in this region are waiting point nuclei for rp-process nucleosynthesis [15] and hence they are of astrophysical interest. The recent development of the recoil-β-tagging technique provides a tool to study medium-mass nuclei around

the $N = Z$ line. In Jyväskylä, excited states of ^{66}As were populated using ^{40}Ca(^{28}Si,pn)^{66}As fusion-evaporation reaction at beam energies of 83 MeV and 75 MeV. Also in this experiment half-lives and ordering of the two known isomeric states (5^+ at 1354 keV and 9^+ at 3021 keV) have been determined with improved accuracy [2].

The deformed shell model (DSM), based on Hartree-Fock (HF) deformed intrinsic states with angular momentum projection and band mixing, is established to be a good model to describe the properties of nuclei in the mass range A=60-100. Also, for N=Z odd-odd nuclei, methods for isospin projection within DSM are developed and applied. See [16] for details regarding DSM and it is found to be quite successful in describing spectroscopic properties, double beta decay half-lives, $\mu - e$ conversion in the field of the nucleus and so on. Following these, in the present paper presented are results of two investigations using DSM. In the first application, recent data [2] for the heavy N=Z nucleus ^{66}As are analyzed using DSM with isospin projection. Secondly, DSM is employed to calculate the detection rates for the lightest supersymmetric particle (a dark matter candidate) with ^{73}Ge as the detector. These are described in Sections 2 and 3 respectively. Finally Section 4 gives conclusions.

2 DSM Results for Spectroscopic Properties of ^{66}As

Calculations are performed in the model space consisting of $2p_{3/2}$, $1f_{5/2}$, $2p_{1/2}$ and $1g_{9/2}$ orbits, with ^{56}Ni as the inert core. For ^{66}As nucleus, Figure 1(a) gives the HF single particle (sp) spectrum (the states are labeled by $|k_\alpha\rangle$ where the α label distinguishes different states with the same k value) for both prolate and oblate solution obtained using the jj44b interaction given in [17]. The prolate state is more bound compared to the oblate intrinsic state by more than 1 MeV. In the prolate case, two protons and two neutrons occupy the lowest $k = (1/2^-)_1$ sp state forming an alpha particle like structure and it has $T = 0$. Similarly, the next $k = 1/2^-$ state is filled by two protons and two neutrons and the last unpaired proton and neutron occupying the lowest $k = 3/2^-$ state. Then, the isospin of the nucleus is determined by these last proton and neutron. The total isospin for the configuration shown in Figure 1(a) is $T = 0$ as the odd proton and odd neutron, for $K = 3^+$, form a symmetric pair in the k-space (here and elsewhere in this paper symmetry in k-space means symmetry in space-spin co-ordinates as k contains both space (orbital) and spin co-ordinates). Particle-hole excitations over the lowest HF intrinsic state (from both prolate and oblate solutions) generate excited HF intrinsic states.

By making particle-hole excitations for the six nucleons out side the lowest k orbit, we have considered 114 configurations shown in Table 1. Out of these, 78 configurations are of prolate shape and 36 oblate shape. Since the lowest oblate configuration lies more than one MeV higher compared to the lowest prolate configuration, we have considered fewer oblate configurations. For the intrinsic states labeled 1-26 with prolate shape in Table 1, the isospin is determined by

Table 1. Prolate (P) and oblate (O) intrinsic states (configurations) used for ^{66}As in the DSM calculation. For each of these, the total K value and isospin T are given in the Table. Superscript $(2p, 2n)$ implies that the orbit is occupied by two protons and two neutrons and similarly the superscript (p, n). In addition, the superscripts $p(n)$ and $n(p)$ imply that the orbit(s) is(are) alternatively occupied by a proton and a neutron or a neutron and a proton. Note that the entries with a $*$ correspond to four particle configurations and those with $**$ correspond to six particle configurations. Similarly, p^- is proton hole and n^- is neutron hole. Note that $X = (1/2^-)_1^{2p,2n}$ and $Y = (3/2^-)_1^{2p,2n}$ in the table.

No.	shape	K	T	Configuration
1.	P	3^+	0	$X\,(1/2^-)_2^{2p,2n}(3/2^-\uparrow)_1^{p,n}$
2,3.	P	0^+	$0,1$	$X\,(1/2^-)_2^{2p,2n}(3/2^-\uparrow)_1^{p(n)}(3/2^-\downarrow)_1^{p(n)}$
4.	P	1^+	0	$X\,(1/2^-)_2^{2p,2n}(1/2^+\uparrow)_1^{p,n}$
5,6.	P	0^+	$0,1$	$X\,(1/2^-)_2^{2p,2n}(1/2^+\uparrow)_1^{p(n)}(1/2^+\downarrow)_1^{p(n)}$
7,8.	P	2^+	$0,1$	$X\,(1/2^-)_2^{2p,2n}(3/2^+\uparrow)_1^{p(n)}(1/2^+\uparrow)_1^{n(p)}$
9,10.	P	1^+	$0,1$	$X\,(1/2^-)_2^{2p,2n}(3/2^+\uparrow)_1^{p(n)}(1/2^+\downarrow)_1^{n(p)}$
11,12.	P	3^+	$0,1$	$X\,(1/2^-)_2^{2p,2n}(3/2^-\uparrow)_1^{p(n)}(3/2^-\uparrow)_2^{n(p)}$
13,14.	P	0^+	$0,1$	$X\,(1/2^-)_2^{2p,2n}(3/2^-\uparrow)_1^{p(n)}(3/2^-\downarrow)_2^{n(p)}$
15,16.	P	0^+	$0,1$	$X\,(1/2^-)_2^{2p,2n}(3/2^-\uparrow)_2^{p(n)}(3/2^-\downarrow)_1^{n(p)}$
17.	P	1^+	0	$X\,(3/2^-)_2^{2p,2n}(1/2^-\uparrow)_2^{p,n}$
18,19.	P	0^+	$0,1$	$X\,(3/2^-)_2^{2p,2n}(1/2^-\uparrow)_2^{p(n)}(1/2^-\downarrow)_2^{p(n)}$
20.	P	1^+	0	$X\,(3/2^-)_2^{2p,2n}(1/2^+\uparrow)_1^{p,n}$
21,22.	P	0^+	$0,1$	$X\,(3/2^-)_2^{2p,2n}(1/2^+\uparrow)_1^{p(n)}(1/2^+\downarrow)_1^{p(n)}$
23,24.	P	1^+	$0,1$	$X\,(1/2^-\downarrow)_2^{p^-(n^-)}(3/2^-\uparrow)_1^{p^-(n^-)}$
25,26.	P	2^+	$0,1$	$X\,(1/2^-\uparrow)_2^{p^-(n^-)}(3/2^-\uparrow)_1^{p^-(n^-)}$
27-32.	P*	1^+	$0,1,2$	$X\,(1/2^-\downarrow)_2^{p^-(n^-)}[(3/2^-)_1(3/2^-\uparrow)_2]^{p,n,p(n)}$
33-38.	P*	2^+	$0,1,2$	$X\,(1/2^-\uparrow)_2^{p^-(n^-)}\left[(3/2^-)_1(3/2^-\uparrow)_2\right]^{p,n,p(n)}$
39-58.	P**	0^+	$0,1,2,3$	$X\,[(1/2^-)_2(3/2^-)_1(3/2^-)_2]^{3p,3n}$
59-78.	P**	0^+	$0,1,2,3$	$X\,[(1/2^-)_2(3/2^-)_1(1/2^+)_1]^{3p,3n}$
79.	O	1^+	0	$Y\,(5/2^-)_1^{2p,2n}(1/2^-\uparrow)_1^{p,n}$
80,81.	O	0^+	$0,1$	$Y\,(5/2^-)_1^{2p,2n}(1/2^-\uparrow)_1^{p(n)}(1/2^-\downarrow)_1^{n(p)}$
82.	O	5^+	0	$Y\,(1/2^-)_1^{2p,2n}(5/2^-\uparrow)_1^{p,n}$
83,84	O	0^+	$0,1$	$Y\,(1/2^-)_1^{2p,2n}(5/2^-\uparrow)_1^{p(n)}(5/2^-\downarrow)^{n(p)}$
85.	O	9^+	0	$Y\,(1/2^-)_1^{2p,2n}(9/2^+\uparrow)_1^{p,n}$
86,87.	O	0^+	$0,1$	$Y\,(1/2^-)_1^{2p,2n}(9/2^+\uparrow)_1^{p(n)}(9/2^+\downarrow)^{n(p)}$
88.	O	9^+	0	$Y\,(5/2^-)_1^{2p,2n}(9/2^+\uparrow)_1^{p,n}$
89,90.	O	0^+	$0,1$	$Y\,(1/2^-)_1^{2p,2n}(9/2^+\uparrow)_1^{p(n)}(9/2^+\downarrow)^{n(p)}$
91-92.	O	2^+	$0,1$	$Y\,(1/2^-\downarrow)_2^{p^-(n^-)}(5/2^-\uparrow)_1^{p^-(n^-)}$
93,94.	O	3^+	$0,1$	$Y\,(1/2^-\uparrow)_2^{p^-(n^-)}(5/2^-\uparrow)_1^{p^-(n^-)}$
95-114.	O**	0^+	$0,1,2,3$	$Y\,[(1/2^-)_1(5/2^-)_1(9/2^+)_1]^{3p,3n}$

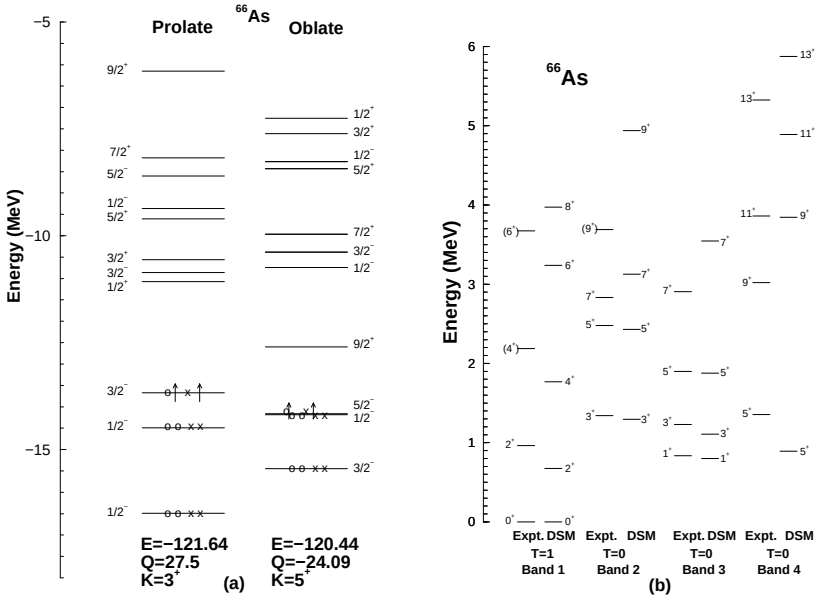

Figure 1. (a) The spectra of sp states for the lowest energy prolate and oblate intrinsic HF configurations for ^{66}As. Protons are represented by circles and the neutrons by crosses. The HF energy in MeV and the quadrupole moment in the units of square of oscillator length parameter are also shown. (b) Comparison of deformed shell model results with experimental data [2] for different bands with jj44b interaction. The band numbers shown in the figure are according to Ref. [2]. Shell model results are obtained using the same jj44b interaction by P.C. Srivastava for this nucleus [21]. For the levels in Band 1, with J^π values in the same order as in the figure, the SM energies are 0.0, 0.899, 2.273, 4.034 and 5.124 MeV respectively. Similarly, for Band 2 members they are 0.889, 2.263, 3.585 and 4.163 MeV, for Band 3 they are 0.426, 0.739, 1.568 and 2.972 MeV and for Band 4 they are 0.985, 1.958, 3.045 and 4.799 MeV respectively.

the last proton and last neutron. When they are in the same orbit with spin up, uniquely $T = 0$. In other situations, it is possible to have both symmetric and antisymmetric spatial configurations giving $T = 0$ and $T = 1$ states respectively as shown in Table 1. With oblate shape we have similar np configurations for intrinsic states labeled 79-94. In addition, with prolate shape a proton or a neutron from the $(1/2^-)_2$ orbit can be promoted to the $(3/2^-)_2$ orbit. Then we have a proton or neutron hole in the $(1/2^-)_2$ orbit. This excited configuration is effectively a four particle (two proton and two neutron) configuration giving six intrinsic states. Constructions of good isospin states from these six states is described in [19]. Projection of isospin from the four particle configurations gives two $T = 0$ states, three $T = 1$ states and one $T = 2$ state. States labeled 27-32 and 33-38 belong to this class. For prolate case, we have also considered configurations with a $(3p, 3n)$ system distributed in six orbits. These six par-

ticle configurations are labeled 39-58 and 59-78 in Table 1. In this situation, distributing in all possible ways the three protons and three neutrons will give twenty different configurations and then isospin projection gives five $T = 0$, nine $T = 1$, five $T = 2$ and one $T = 3$ intrinsic states. The details regarding isospin projection for the six particle case is given in Ref. [20]. For oblate shape, we have considered one set of six particle configurations and they are labeled 95-114 in Table 1. Combining all these, we have a total of forty four $T = 0$ configurations and fifty $T = 1$ configurations (in addition there are seventeen $T = 2$ configurations and three $T = 3$ configurations but they are not relevant as experimental data contains only $T = 1$ and $T = 0$ levels). We project out good angular momentum states from different intrinsic states of a given isospin and then perform band mixing calculations. The resulting spectrum for $T = 0$ and $T = 1$ bands are compared with experiment in Figure 1(b).

The DSM calculated $T = 1$ band agrees reasonably well with experiment. Except for the $2^+ \rightarrow 0^+$ separation, the relative spacing of all other levels are reasonably reproduced. The $T = 1$ levels up to $J = 6^+$ mainly originate from the lowest $T = 1$ intrinsic state generated by the antisymmetric combination of the configurations No. $(2, 3)$ in Table 1. Hence, there is no change in the collectivity up to $J = 6^+$. The shell model (SM) as well as the DSM predicts the B(E2) values for the transition $8^+ \rightarrow 6^+$ to be very small. For example, the B(E2) ratios $B(E2, I \rightarrow I - 2)\ /B(E2, I - 2 \rightarrow I - 4)$ with I=4, 6, 8 are 1.22, 0.97 and 0.001 in DSM. The corresponding ratios for shell model are 1.29, 1.09 and 0.001. The occupancy of the $1g_{9/2}$ orbit obtained from SM does not change much up to spin $T = 1, J = 6^+$ and is about 0.64 for both protons and neutrons. However, as we go to $T = 1, 8^+_1$ level, there is a dramatic change in the occupancy which is 1.05 in SM. Thus, shell model predicts the structure of the $T = 1, 8^+_1$ level to be quite different from that of the other $T = 1$ levels lying below. As a result, the $B(E2)$ transition probability from $T = 1, 8^+$ to $T = 1, 6^+$ is small. This is in agreement with the conclusion drawn from the DSM calculation which predicts that the structure of the $T = 1, 8^+_1$ level to be a quite different from that of the $T = 1, 6^+_1$ level. This level originates from the $T = 1$ projected intrinsic state in which three protons and three neutrons are distributed in six single particle orbitals with configuration that corresponds to No. 59-78 in Table 1. This configuration has a proton and a neutron in $g_{9/2}$ orbit just the occupancy given by SM. With the structure of the $T = 1, 8^+_1$ level being quite different from the $T = 1, 6^+_1$, its E2 transition probability to $T = 1, 6^+_1$ level is also small in DSM just as in SM.

Coming to the $T = 0$ bands, it is seen from Figure 1(b) that the DSM calculated spectra for the first two $T = 0$ bands (band 2 and band 3 in the figure) agree reasonably well with experiment (also with shell model). The levels 3^+, 5^+, 7^+ and 9^+ of band 2 with $T = 0$ mainly originate from the lowest T=0 intrinsic state No. 1 given in Table 1. However, the mixing from other intrinsic states increases for the higher spin states. The band 3 with $T = 0$ consists of 1^+, 3^+, 5^+ and 7^+ levels. All these levels except 7^+ level are found to have similar

structure. They mainly originate from the lowest T=0 intrinsic state No. 1 in Table 1 and from the symmetric combination of the intrinsic states No. $(2,3)$ given in Table 1. Thus, both these two $T = 0$ bands exhibit quasi-deuteron structure above a ^{64}Ge core.

The band 4 (also with $T = 0$) consists of a level with spin 5^+ and in DSM this level is essentially generated by the oblate configuration $(3/2^-)_1^{2p,2n}$ $(1/2^-)_1^{2p,2n}(5/2^- \uparrow)_1^{p,n}$ (No. 82 in Table 1). The calculated $B(E2)$'s from this level to the lower 3^+ levels of band 2 and band 3 are very small. Thus, this level is an isomeric state obtained from the totally aligned $^1f_{5/2}\, np$ configuration consistent with the claim in [2]. Also, the structure of this 5^+ level is similar to the 7^+ level of band 3. This is possibly the reason why in the experiment reported in [2], a large transition strength between these two levels is seen. The other levels of this band are 9^+, 11^+ and 13^+. The 9^+ energy from DSM is higher than the experimental value by about 1 MeV. However the relative spacings are quite well reproduced. The 9^+ level originates from the oblate intrinsic state No. 85 given in Table 1 with configuration $(3/2^-)_1^{2p,2n}(1/2^-)_1^{2p,2n}(9/2^+ \uparrow)_1^{p,n}$. It has also strong mixing from the prolate intrinsic states No. (5,6), (7,8) and (9,10) given in Table 1. The calculated B(E2) values from this level to the lower 7^+ levels of bands 2 and 3 are very small. Thus, this level is predicted to be a isomeric state with totally aligned np pair in $^1g_{9/2}$ orbit as the dominant structure. The yrast 11^+ and 13^+ levels in DSM do not have the same structure and the levels with aligned structure appear at much higher energies and they are not shown in the figure. Hasegawa et al [22] have performed a spherical shell model study using an extended pairing plus quadrupole-quadrupole Hamiltonian and they also found the 9^+ levels to be a isomeric state as in DSM. Cranked Nilsson-Strutinsky calculations and SM also predict a band 4 with 9^+, 11^+ and 13^+ (also higher J^π) with totally aligned pn pair in $^1g_{9/2}$ orbit [21]. Thus, ^{66}As also shows spin aligned np isoscalar pair phase as seen before in ^{92}Pd [14].

It is important to add that the inclusion of six particle configurations on one hand and mixing of several intrinsic states with prolate and oblate shapes on the other, are responsible for the good agreements seen for various bands generated by DSM (the band 5 with three levels identified in experiment was not discussed here as the assignment of both the angular momentum and parity of these levels is uncertian). Also, the present calculations show considerable improvements over the previous DSM results [18] where only limited number of two particle configurations are included and a realistic G-matrix interaction with a phenomenologically adjusted monopole part as given by the Madrid-Strasbourg group has been used.

3 DSM Application to Dark Matter: Elastic Scattering of LSP from ^{73}Ge

There is overwhelming evidence for the existence of dark matter in the universe [23, 24]. Up to now, the nature of this matter remains a mystery. In recent years,

there have been considerable theoretical and experimental efforts to detect the cold dark matter (CDM) which is thought to be the dominant component of the dark matter [25]. In the highly favored Super Symmetric (SUSY) model, the most natural non-baryonic CDM candidate is the lightest supersymmetric particle (LSP) which is non-relativistic.

Since the LSP (represented by χ) interacts very weakly with matter, its detection is quite difficult. One possibility to detect LSP is through its elastic scattering from nuclei. Inelastic channels are not excited since the energy is too low to excite the nucleus and hence the cross section should be negligible. On the other hand exotic WIMPs (weakly interacting massive particles) can lead to large nucleon spin induced cross sections which in turn can lead to non-negligible probability for inelastic WIMP-nucleus scattering [25]. Here we will consider only the elastic channels. First we will discuss briefly the formulation for LSP-nucleus scattering cross section calculation and the related aspects of DSM. Next, results of the application to ^{73}Ge detector are described.

3.1 Formulation

Defining the dimensionless quantity $u = q^2b^2/2 = M_A b^2 \overline{Q}$ where q represents the momentum transfer to the nuclear target, b is the nuclear harmonic oscillator size parameter, $\overline{Q}$ is the energy transfer to the nucleus and M_A is the nuclear mass, the LSP-nucleus differential cross section in the laboratory frame is given by [26, 27],

$$\frac{d\sigma(u,v)}{du} = \frac{1}{2}\,\sigma_0 \left(\frac{1}{m_p b}\right)^2 \frac{c^2}{v^2}\,\frac{d\sigma_{AS}(u,v)}{du}\;; \tag{1}$$

$$\frac{d\sigma_{AS}(u,v)}{du} = \left[f_A^0\Omega_0(0)\right]^2 F_{00}(u) + 2f_A^0 f_A^1 \Omega_0(0)\Omega_1(0)F_{01}(u) + \left[f_A^1\Omega_1(0)\right]^2 F_{11}(u) + M^2\;. \tag{2}$$

In the above, m_p is the mass of the proton, v is the LSP velocity with respect to the earth and $\sigma_0 = 0.77 \times 10^{-38}$ cm^2. If the proton and neutron form factors $F_Z(u)$ and $F_N(u)$ are different, then

$$M^2 = \left(f_S^0\,\left[ZF_Z(u) + NF_N(u)\right] + f_S^1\,\left[ZF_Z(u) - NF_N(u)\right]\right)^2\;. \tag{3}$$

Here, f_A^0 and f_A^1 represent isoscalar and isovector parts of the axial vector current and similarly f_S^0 and f_S^1 represent isoscalar and isovector parts of the scalar current. These nucleonic current parameters depend on the specific SUSY model

employed. The spin structure functions $F_{\rho\rho'}(u)$ with ρ, ρ' = 0,1 are defined as

$$F_{\rho\rho'}(u) = \sum_{\lambda,\kappa} \frac{\Omega_{\rho}^{(\lambda,\kappa)}(u)\Omega_{\rho'}^{(\lambda,\kappa)}(u)}{\Omega_{\rho}(0)\Omega_{\rho'}(0)} \; ;$$
$$\Omega_{\rho}^{(\lambda,\kappa)}(u) = \sqrt{\frac{4\pi}{2J_i+1}} \langle J_f \| \sum_{j=1}^{A} [Y_\lambda(\Omega_j) \otimes \sigma(j)]_\kappa \, j_\lambda(\sqrt{u}\, r_j) \times \omega_\rho(j) \| J_i \rangle \tag{4}$$

with $\omega_0(j) = 1$ and $\omega_1(j) = \tau(j)$; note that $\tau = +1$ for protons and -1 for neutrons. Here Ω_j is the solid angle for the position vector of the j-th nucleon and j_λ is the spherical Bessel function. The static spin matrix elements are defined as $\Omega_\rho(0) = \Omega_\rho^{(0,1)}(0)$. As has been described in [26], the LSP detection rate is given by the simple expression,

$$R_0 = 8.9 \times 10^7 \times \frac{\sigma_{AS}(v_{esc})}{A \; m_\chi[GeV](m_p b)^2} [yr^{-1} kg^{-1}] \; . \tag{5}$$

Note that $v_{esc} = 625$ km/s is the escape velocity of the LSP from the milkyway and the LSP mass m_χ is taken to be 110 GeV. The $\sigma_{AS}(v_{esc})$ is obtained using Eq. (2) and the Maxwell velocity distribution (for v). In the integral over u, the lower limit involves the detector threshold energy Q and the upper limit involves v_{esc}.

The nuclear structure part is in the spin structure functions and the form factors. It is here DSM is used. The reduced matrix element appearing in Eq. (4) can be evaluated in DSM. Here we need the sp matrix elements of the operator of the form $t_\nu^{(l,s)J}$ and these are given by,

$$\langle n_i l_i j_i \| \hat{t}^{(l,s)J} \| n_k l_k j_k \rangle = \sqrt{(2j_k+1)(2j_i+1)(2J+1)(s+1)(s+2)}$$
$$\left\{ \begin{array}{ccc} l_i & 1/2 & j_i \\ l_k & 1/2 & j_k \\ l & s & J \end{array} \right\} \langle l_i \| \sqrt{4\pi} Y^l \| l_k \rangle \; \langle n_i l_i \| j_l(kr) \| n_k l_k \rangle \; . \tag{6}$$

In the above equation, $\{--\}$ is the nine-j symbol.

3.2 Results and discussion

Above formulation is used for LSP detection rates for scattering from ^{73}Ge with DSM for the nuclear structure part. The sp orbits employed are $^2p_{3/2}$, $^1f_{5/2}$, $^2p_{1/2}$ and $^1g_{9/2}$ with^{56}Ni core and the sp energies are taken as 0.0, 0.78, 1.08 and 4.90 MeV respectively. The effective interaction used is the modified Kuo interaction [28]. The HF sp spectrum is shown in Figure 2a. For ^{73}Ge, the experimental energy spectrum has positive and negative parity levels at low energy. Hence, for band mixing in DSM three intrinsic states with positive parity and three with negative parity are considered. The final energy spectrum and

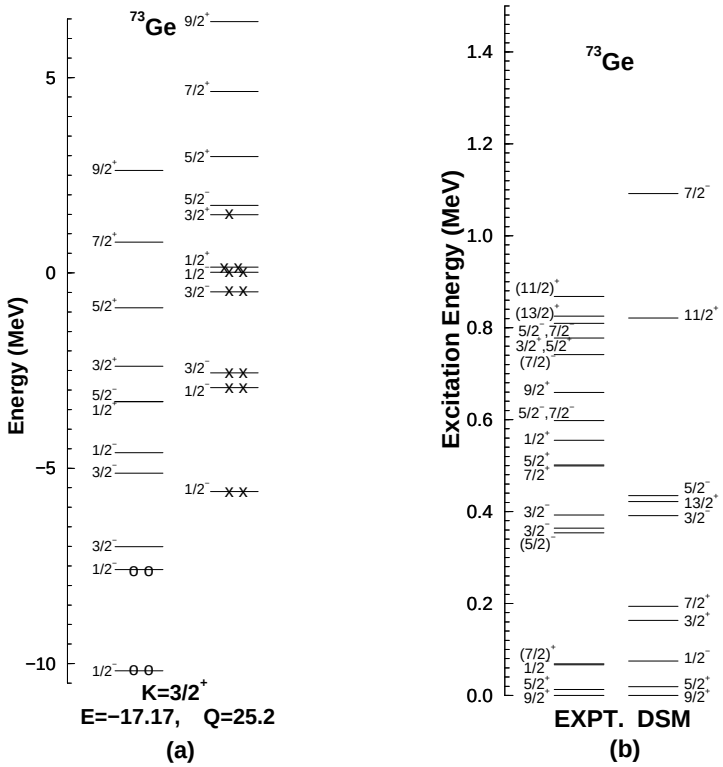

Figure 2. (a) The lowest prolate HF sp spectrum for ^{73}Ge. The HF energy E in MeV and the mass quadrupole moment Q in units of the square of the oscillator length parameter b are also given. Protons are represented by circles and neutrons by crosses. (b) Theoretical (DSM) and experimental (EXPT) spectra of ^{73}Ge. Data are taken from [29].

its comparison with experiment is shown in Figure 2b. Since spin contributions play an important role in the the calculation of the decay rates, the magnetic moment is decomposed into orbital and spin parts for this nucleus. The DSM value for the magnetic moment (using bare values for the g-factors) is $-0.811\ \mu_N$ and it is close to experimental value $-0.879\ \mu_N$ [29]. The matrix elements of the proton orbital and spin angular momenta are 0.581 and -0.001 respectively and similarly, for neutron the values are 3.558 and 0.362 respectively.

Depending on the SUSY parameters, the detection rate varies widely as described in [26]. The same feature is also found in DSM. The values of the parameters f_A^0, f_A^1, f_S^0 and f_S^1 are taken from [30] and they are 3.55×10^{-2}, 5.31×10^{-2}, 8.02×10^{-4} and $-0.15 \times f_S^0$ respectively. For ^{73}Ge, DSM gives the values of Ω_0 and Ω_1 to be 0.798 and -0.803. These values are smaller than those quoted in [26], where a quasi-particle-phonon model (QPM) is used, by 20 to 30 percent. The spin structure functions which do not depend on the oscillator

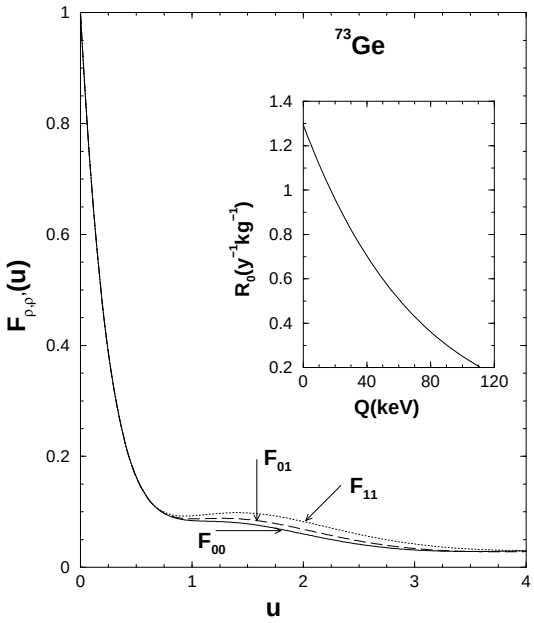

Figure 3. Spin structure functions for ^{73}Ge as a function of momentum transfer u. Shown in the insect figure is LSP detection rate as a function of Q, the detector threshold energy.

length parameter are plotted in Figure 3. The structure functions for ^{73}Ge are similar to those obtained using QPM in [26]. Ressell *et al.* [31] calculated $S_{\rho\rho'}$, that are related to the spin structure functions defined above, using shell model. The spin structure functions from DSM are similar to their values. Following these, the detection rate as a function of Q is obtained using Eq. (5) and the results are shown in Figure 3. Results in the figure show that ^{73}Ge is a good detector for detecting dark matter.

4 Conclusions

Applications of DSM to two current problems of interest in nuclear structure are presented in this paper. They are: (i) analysis of recent data on low-lying $T = 1$ and $T = 0$ bands in the heavy N=Z nucleus ^{66}As; (ii) detections rates for the light supersymmetric particle, a dark matter candidate, with ^{73}Ge as the detector. In future heavy N=Z nuclei will be further analyzed to bring out isoscalar pairing vs isovector pairing in these nuclei by using extended pairing plus quadrupole-quadrupole Hamiltonian of the Sofia group [32] and comparing the results of DSM obtained with this interaction with those using realistic interactions. In addition, in the topic of dark matter, DSM will be employed to study inelastic

(spin dependent) WIMP-nucleus scattering in ^{83}Kr and this is unlike LSP that involves only elastic scattering.

Acknowledgments

The authors are thankful to P.C. Srivastava for useful correspondence. R. Sahu is thankful to SERB of Department of Science and Technology (Government of India) for financial support.

References

[1] H.M. David *et al.*, *Phys. Lett. B* **726** (2013) 665-669.
[2] P. Ruotsalainen *et al.*, *Phys. Rev. C* **88** (2013) 024320/1-16.
[3] D.G. Jenkins *et al.*, *Phys. Rev. C* **65** (2002) 064307/1-16.
[4] D. Rudolph *et al.*, *Phys. Rev. Lett.* **76** (1996) 376-379.
[5] B.S. Narasingh *et al.*, *Phys. Rev. C* **75** (2007) 061301(R)/1-4.
[6] A.B. Garnsworthy *et al*, *Phys. Lett. B* **660** (2008) 326-330.
[7] K. Starosta *et al.*, *Phys. Rev. Lett.* **99** (2007) 042503/1-4.
[8] S.M. Fischer *et al.*, *Phys. Rev. Lett.* **84** (2000) 4064-4067.
[9] G. de Angelis *et al.*, *Phys. Lett. B* **415** (1997) 217-222.
[10] H. Iwasaki *et al.*, *Phys. Rev. Lett.* **112** (2014) 142502/1-5.
[11] J. A. Briz *et al.*, *Phys. Rev. C* **92** (2015) 054326/1-10.
[12] A. Lemasson *et al.*, *Phys. Rev. C* **85** (2012) 041303(R)/1-4.
[13] C.J. Lister *et al.*, *Phys. Rev. Lett.* **59** (1987) 1270-1273.
[14] B. Cederwall *et al.*, *Nature* **469** (2011) 68i-71.
[15] J. Pruet and G. M. Fuller, *Astrophys. J. Suppl. Ser.* **149** (2003) 189-204.
[16] V.K.B. Kota and R. Sahu, *Structure of Medium Mass Nuclei: Deformed Shell Model and Spin-isospin Interacting Boson Model* (CRC Press, Taylor and Francis group, Florida), in press.
[17] B.A. Brown and A.F. Lisetskiy (unpublished); see also endnote (28) in B. Cheal *et al.*, *Phys. Rev. Lett.* **104** (2010) 252502/1-5.
[18] R. Sahu and V.K.B. Kota, *Phys. Rev.* **C 66** (2002) 024301/1-6.
[19] R. Sahu and V.K.B. Kota, *Eur. Phys. J. A* **24** (2005) 5-11.
[20] V.K.B. Kota and R. Sahu, in: *Proceedings of the Workshop on Frontiers in Gamma ray Spectroscopy (FIG09)*, Edited by R. Palit and R. Pillay, (TIFR, Mumbai, India, 2011), p. 83-93.
[21] P.C. Srivastava, Private communication.
[22] M. Hasegawa, Y. Sun, K. Kaneko and T. Mizusaki, *Phys. Lett. B* **617** (2005) 150-156.
[23] G. Jungman, M. Kamionkowski and K. Griest, *Phys. Rep.* **267** (1996) 195-373.
[24] D. Majumdar, *Dark Matter: An Introduction* (CRC press, Taylor and Francis group, Florida, 2014).
[25] J.D. Vergados, F.T. Avignone III, P. Pirinen, P.C. Srivastava, M. Kortelainen and J. Suhonen, *Phys. Rev. D* **92** (2015) 015015/1-13.

[26] E. Holmlund, M. Kortelainen, T.S. Kosmas, J. Suhonen and J. Toivanen, *Phys. Lett. B* **584** (2004) 31-39.

[27] P.C. Divari, T.S. Kosmas, J.D. Vergados and L.D. Skouras, *Phys. Rev. C* **61** (2000) 054612/1-12.

[28] D.P. Ahalpara, K.H. Bhatt and R. Sahu, *J. Phys. G: Nucl. Phys.* **11** (1985) 735-744.

[29] `http://www.nndc.bnl.gov/ensdf`

[30] J.D. Vergados, J. Phys. G: *Nucl. Part. Phys.* **22** (1996) 253-272.

[31] M. Ted Ressell *et al.*, *Phys. Rev. D* **48** (1993) 5519-5535

[32] K. Drumev, in this proceedings.